Detection of a magnetic bead by hybrid nanodevices using scanning gate microscopy

Cite as: AIP Advances **6**, 056502 (2016); https://doi.org/10.1063/1.4943147
Submitted: 06 November 2015 . Accepted: 07 December 2015 . Published Online: 29 February 2016

H. Corte-León, P. Krzysteczko, F. Marchi, J.-F. Motte, A. Manzin, H. W. Schumacher, V. Antonov, and O. Kazakova

Detection of a magnetic bead by hybrid nanodevices using scanning gate microscopy

H. Corte-León,[1,2,a] P. Krzysteczko,[3] F. Marchi,[4] J.-F. Motte,[4] A. Manzin,[5]
H. W. Schumacher,[3] V. Antonov,[2] and O. Kazakova[1]
[1]*National Physical Laboratory, Teddington, TW11 0LW, United Kingdom*
[2]*Royal Holloway University of London, Egham, TW20 0EX, United Kingdom*
[3]*Physikalisch-Technische Bundesanstalt, Braunschweig, D-38116, Germany*
[4]*Univ. Grenoble Alpes, Inst. NEEL, Grenoble, F-38042, France*
[5]*Istituto Nazionale di Ricerca Metrologica, Torino, I-10135, Italy*

(Presented 15 January 2016; received 6 November 2015; accepted 7 December 2015;
published online 29 February 2016)

Hybrid ferromagnetic(Py)/non-magnetic metal(Au) junctions with a width of 400 nm are studied by magnetotransport measurements, magnetic scanning gate microscopy (SGM) with a magnetic bead (MB) attached to the probe, and micromagnetic simulations. In the transverse geometry, the devices demonstrate a characteristic magnetoresistive behavior that depends on the direction of the in plane magnetic field, with minimum/maximum variation when the field is applied parallel/perpendicular to the Py wire. The SGM is performed with a NdFeB bead of 1.6 μm diameter attached to the scanning probe. Our results demonstrate that the hybrid junction can be used to detect this type of MB. A rough approximation of the sensing volume of the junction has the shape of elliptical cylinder with the volume of ~1.51 μm^3. Micromagnetic simulations coupled to a magnetotransport model including anisotropic magnetoresistance and planar Hall effects are in good agreement with the experimental findings, enabling the interpretation of the SGM images. [http://dx.doi.org/10.1063/1.4943147]

I. INTRODUCTION

Detection and manipulation of magnetic beads (MBs) using ferromagnetic nanodevices open the possibility of integrating several laboratory functions into a single chip to achieve automation and high-throughput screening (*i.e.* Lab-on-a-Chip) for biomedical applications.[1,2] In particular, magnetoresistive effects such as anisotropic magnetoresistance (AMR), or planar Hall effect (PHE), in combination with domain wall (DW) based technology, allow manipulation of MBs and their electrical detection.[3–9]

In a typical detection experiment, a MB suspended in a fluid is attracted by the magnetic force due to the stray field gradient generated by a DW[1] pinned inside a nanowire. Detection of the MB can be achieved by tracking the DW pinning/depinning process using longitudinal resistance measurements (AMR configuration).[4] However, the intrinsic changes in the resistance due to the presence/absence of the DW are relatively small, *i.e.* typically ~0.2%.[10] Moreover, longitudinal resistance measurements are highly affected by the stochastic DW pinning/depinning process. In order to overcome these problems without modifying the basic elements, sensors based on ferromagnetic crosses (PHE configuration) have been proposed.[3,11–20] However, such devices still have to deal with DW pinning at the cross corners.[20–22] An alternative solution exploited here is a sensor based on transversal resistance measurements in a nanowire using an overlaying metallic non-magnetic wire. In particular, we propose a nanoscale hybrid ferromagnetic (Py)/non-magnetic metal (Au) junction as a single nanoparticle detector. In this geometry, a straight Py nanowire

[a]Electronic mail: hector.corte@npl.co.uk

is a track for DW propagation and an active sensing element with no pinning sites, whereas the Au overlaying nanowire is used for the electrical signal detection. The sensitivity of this nanostructured device has been studied by performing magnetotransport measurements, magnetic scanning gate microscopy (SGM) with a MB attached to the scanning probe,[23,24] and coupled micromagnetic-magnetotransport simulations.

The magnetotransport measurements performed on the hybrid junction demonstrate a good sensitivity to small in-plane fields in the range of few mT. The SGM mapping obtained with a NdFeB MB attached to the probe demonstrates the possibility of single ferromagnetic MB detection using hybrid junctions. Furthermore, we define the active sensing volume (*i.e.* the volume where the center of the MB has to be placed in order to be detected by the given sensor). Micromagnetic simulations combined to a magnetotransport model show a good agreement with SGM results, demonstrating that the output signal is dominated by the PHE.

II. EXPERIMENTAL AND MODELLING METHODS

Magnetic L-shaped nanodevices were fabricated from a continuous polycrystalline Py/Pt film (t = 25/2 nm). Each device has two arms of 20 μm in length and 400 nm in width at 90º to each other, forming a square corner with disks of 1 μm in diameter at the end of each arm (Fig. 1(a)).

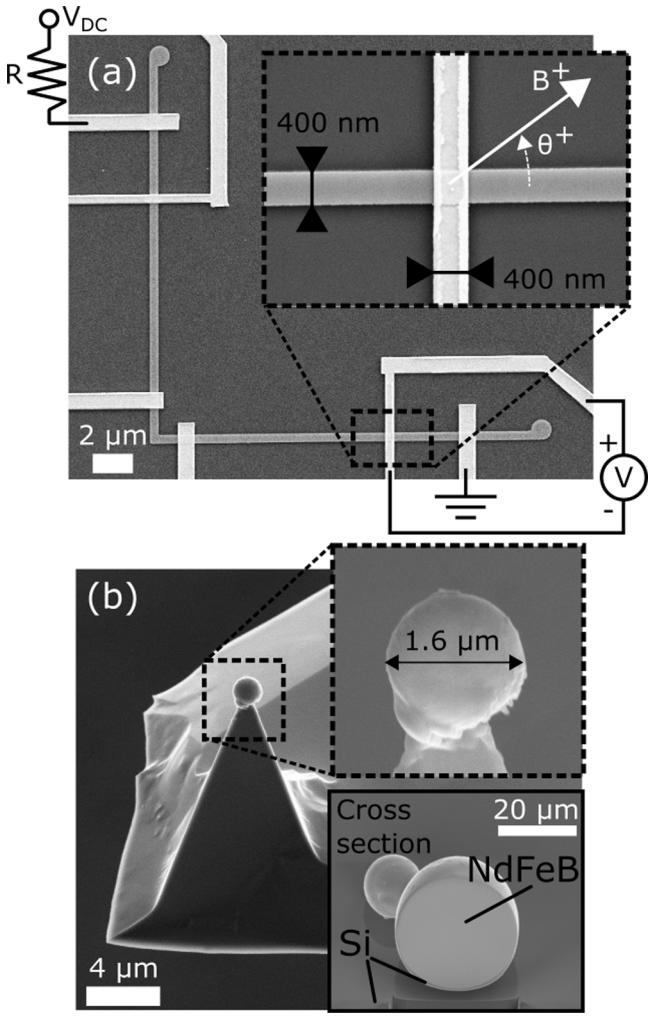

FIG. 1. (a) SEM image of the whole L-shaped device with electrical connections. Inset: hybrid Py/Au junction studied in this work. (b) AFM probe with a NdFeB MB attached. Top inset: magnified image of the MB. Bottom inset: cross section of a large NdFeB MB milled down using FIB.

Gold leads were prepared by sputtering deposition of Ta (~6 nm) and Au (~150 nm). The hybrid cross-shaped junctions, included as part of the design (Fig. 1(a) inset), are composed of a straight 400 nm wide Py wire with an overlaying 400 nm wide Au wire.

The L-shaped Py nanodevices possess 4 well-defined remanent magnetization states,[10] depending on the magnetization spatial distribution along the two arms and the previous field history. These states, which can be tracked by measuring the resistance at the corner,[10] are tail-to-tail DW, head-to-head DW, and two magnetization configurations with no DW. As it was previously demonstrated,[4] all these states are characterized by uniform magnetization distribution along the arms. This allow the Py/Au hybrid junction to be treated as an individual device, where magnetization is uniformly distributed in the Py wire without taking into account the overall geometry.

Magnetotransport measurements are performed using the electrical circuit depicted in Fig. 1(a). For these measurements, the DC voltage (V_{DC} in Fig. 1(a)) is kept at a constant value (V_{DC} = 5 V), while the current through the device, I_{DC} = 103 μA, is fixed by the large value of the resistor, R = 48.7 kΩ. The output voltage at the junction is measured using a nanovoltmeter with 2 PLCs as integration time. A rotating stage allows to apply magnetic field along different directions.

The SPM system (Aura, NT-MDT with home-built transport measurement stage) was used in air and at room temperature for magnetic SGM studies. This system allows application of an in-plane magnetic field during scanning, as well as electrical connections to the sample. In SGM mode, the sample's topography is recorded in non-contact mode during the first scan. Then, during the second scan performed at an elevated height using the previously recorded topography to keep a constant height with the surface, the oscillation amplitude of the probe is set to zero and the transversal resistance at the junction is measured in correspondence to the position of the scanning probe. To minimize the electrostatic interactions, the probe is grounded. The transversal resistance is measured using the same electrical circuit as for the magnetotransport measurements (Fig. 1(a)), but employing an external lock-in amplifier with AC bias current of 100 μA at 44 kHz. This precaution is taken to reduce AC noise introduced by the AFM system which is difficult to filter, once verified that the AC response of the junction at the selected frequency is similar to the DC response.

The modified probes used in SGM (Fig. 1(b)) have been custom-made by removing the apex of a commercial silicon AFM tip (TESPA, Bruker) and placing a MB on the flattened pyramid using a FIB system equipped with micromanipulators.[4] The tip's spring constant (56.29 N/m) and its resonant frequency (351.5 kHz) were measured using the standard thermal tune calibration technique. A high spring constant value is chosen in order to minimize the static bending of the cantilever due to the MB-sample force; in this way, the MB-sample height remains constant all over the SGM scan. The MBs used in this work are commercial magnetic NdFeB microspheres (MQP-S-11-9-20001-070 Isotropic Powder[25]) with diameter of ~1.6 μm (Fig. 1(b) top inset). Considering a remanence magnetization for the powder with value M_r = 57.60 Am^2/kg, and a density of the powder in bulk, ρ = 3600 kg/m^3,[25] the estimated magnetic moment of the MB, assumed as a sphere with 1.6 μm diameter, is m ~4.48 x 10^{-13} Am^2.[26] The coercivity of the NdFeB microspheres is ~840 mT. Prior to the experiment, the microspheres were magnetized by applying a magnetic field of ~2 T perpendicular to the cantilever.

In order to check the homogeneity of the material distribution inside the NdFeB microspheres, a particle of significantly larger diameter than used in this work was selected and milled with FIB (Fig. 2(b) bottom inset). Even the large microsphere appears to be uniform with no cavities, inclusions and visible defects, thus implying homogeneity of smaller beads used in SGM (Si on the bottom side of the MB was deposited from the substrate during the milling process).

The SGM results are interpreted by means of a modeling approach that combines micromagnetic simulations with a magnetotransport model including both AMR and PHE effects. First, the magnetization configuration is calculated with a parallelized micromagnetic solver,[27,28] which time-integrates the Landau-Lifshitz-Gilbert (LLG) equation by means of a norm-conserving scheme based on Cayley transform.[29] Second, at each equilibrium point the spatial distribution of the electric field, expressed as the gradient of scalar potential ϕ, is obtained by numerically solving the following equation

$$\nabla \cdot \left[\overleftrightarrow{\sigma}(\mathbf{r}) \nabla \phi(\mathbf{r}) \right] = 0 \tag{1}$$

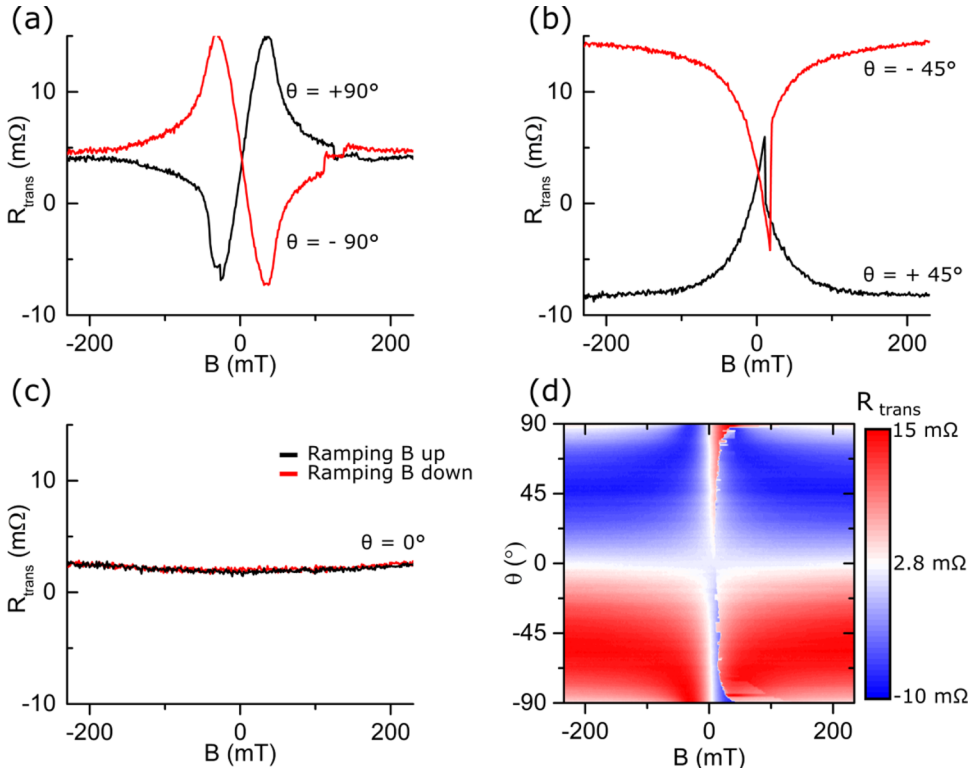

FIG. 2. a-c) Transversal resistance of the hybrid junction when the field is applied at (a) $\theta = \pm 90°$; (b) $\theta = \pm 45°$; (c) $\theta = 0°$. (d) Transversal resistance for different angles of the applied field, $-90° < \theta < +90°$, $\Delta\theta = 0.9°$, when the field is ramped from negative to positive saturating values.

For thin film based nanostructures, the spatially dependent conductivity tensor $\overleftrightarrow{\sigma}(\mathbf{r})$ reduces to

$$\overleftrightarrow{\sigma}(\mathbf{r}) = \frac{1}{\rho_{\parallel}\rho_{\perp}} \begin{bmatrix} \rho_{\parallel} - \Delta\rho \cos^2\eta(\mathbf{r}) & -\frac{1}{2}\Delta\rho \sin 2\eta(\mathbf{r}) \\ -\frac{1}{2}\Delta\rho \sin 2\eta(\mathbf{r}) & \rho_{\parallel} - \Delta\rho \sin^2\eta(\mathbf{r}) \end{bmatrix} \tag{2}$$

where $\Delta\rho = \rho_{\parallel} - \rho_{\perp}$, with $\rho_{\parallel}$ and $\rho_{\perp}$ being the resistivities parallel and orthogonal to the magnetization direction, which forms an angle $\eta(\mathbf{r})$ with respect to x-axis.[17,30,31]

The non-linear equation (1), coupled to *ad hoc* boundary conditions on current contacts and insulating boundaries, is iteratively solved until convergence of conductivity.[32]

In the micromagnetic simulations, the saturation magnetization of Py is fixed to 860 kA/m, the exchange constant to 13pJ/m and the magnetocrysalline anisotropy to zero. In the magnetotransport model, $\rho_{\parallel} = 0.34\ \mu\Omega$m and $\rho_{\perp} = 0.333\ \mu\Omega$m.[33]

The interaction between the device and the NdFeB MB is taken into account by adding to the effective field in the LLG equation the magnetic stray field of the MB, which is approximated as a magnetic dipole located at a height corresponding to the distance between the device surface and the MB barycenter.

III. RESULTS

Experimental results are divided into three parts. First, we perform the electrical characterization of the junction by means of magnetotransport measurements using in-plane applied field. Second, SGM mapping is done at a constant height (h in range 100 – 700 nm), while the magnetization of the Py wire is aligned along two different directions. In this work we demonstrate single MB detection and evaluate contribution of the Py magnetization to the overall signal. This is further supported by micromagnetic-magnetotransport simulations enabling interpretation of SGM images.

Finally, by performing SGM measurements at different heights, the sensing volume of the hybrid junction is estimated.

A. Magnetotransport characterization of the junction

Magnetotransport measurements have been performed using the electrical circuit shown in Fig. 1(a) in presence of an in-plane external magnetic field as indicated in Fig. 1(a) inset. The resulting field dependence of the transversal resistance (*i.e.* transversal voltage divided by the bias current) is shown in Fig. 2. The individual curves for the field ramped from negative to positive saturating values are shown for different angular orientations: $\theta = \pm 90°$, $\pm 45°$ and $0°$ in Figs. 2(a), 2(b) and 2(c), respectively. Fig. 2(d) shows the combined results for all angular orientations between -90° and +90° with a small angular step of 0.9°. As expected from Eq. (2), there is almost no variation in the resistance when the field is applied along the nanowire (Fig. 2(c)), and the variation is maximum in the low field range when the field is perpendicular to the nanowire (Fig. 2(a)). At $\theta = 90°$ (Fig. 2(a)) a linear fitting in the range of -20 mT < B < 20 mT allows to estimate the maximum sensitivity of the junction, S = 0.46 Ω/T. This sensitivity is relatively small when compared to micro-Hall sensors with similar active area.[19,34]

Steps in the transversal resistance correspond to magnetization switching events along the Py wire and propagation of a DW (Figs. 2(a), 2(b)). A summary of angular measurements of the magnetization reversal is presented in Fig. 2(d) where the steps occur at different fields depending on the angular orientation. In addition, Fig. 2(d) demonstrates absence of the DW pinning at the junction, as a DW pinned at the junction would be associated with two steps in the resistance.

It is noteworthy that experimental curves show a constant background resistance of ~2.8 mΩ (Fig. 2), which is associated with the electrical contacts and depends on the width of the overlaying Au wire as well as on the quality of the interface between Au and Py.

B. MB detection experiment

In SGM, first the topography of the sample is recorded in Non-contact mode (Fig. 3(a)), then the probe is retracted and magnetic field is applied to magnetize the device in a set direction. Finally, the probe is brought into the device proximity again and resistance is measured, while the probe moves at a constant height over the surface using the previously recorded topography as a reference, and setting the oscillation amplitude to zero.[23] It is important to note that due to the MB-surface convolution, the topography recorded in Fig. 3(a) shows a junction significantly wider than the one image using SEM (Fig. 1(a)). This convolution effect has a small influence when doing the second pass because of the relative size of the MB compared to the junction.

Results of the transversal resistance mapping when the probe is at 200 nm above the surface are shown in Fig. 3(b). Left and right panels of Fig. 3(b) report the cases of different magnetization orientation along the Py wire (indicated by the green arrow). A cross-section of one of the images (shown in Fig. 4(b) left) demonstrates variations of the magnetoresistance behavior along the Au wire in correspondence of the junction, as also confirmed by simulation results obtained for different distances h between the device surface and the MB bottom (Fig. 4(b) right). Figure 3(b) demonstrates that the presence of the MB produces a detectable signal on the transversal resistance (Fig. 3(b)), hence the junction can be used as a detector, and the direction of the magnetization along the Py nanowire determines the sign of the interaction as follows from Eq. (2). The background resistance Fig. 3(b) also shows that, despite using AC bias signal for this experiment, the resistance is about 2 mΩ even at B = 0, *i.e.* similar to that obtained in the magnetotransport measurements using DC current. It should be also notice here that although MB was magnetized perpendicular to the cantilever, the MB magnetization direction and the sample surface are not exactly perpendicular to each other. This is due to the angle introduced by the tip holder ~15°, the tilt angle of the sample, and the unknown angle introduced by the tip holder support. However, since the SGM images in Fig. 3(b) show a symmetric influence when the MB is one side or the other of the Py, it can be concluded that the magnetization of the MB and the surface are close to be perpendicular to each other.

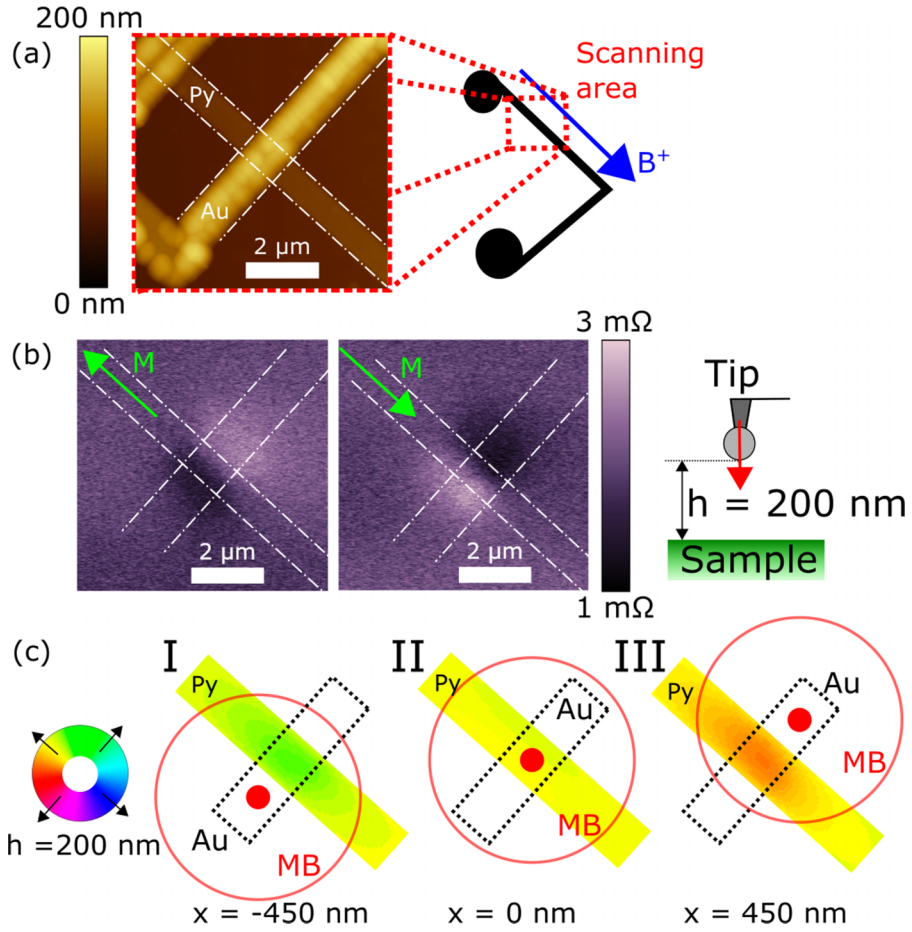

FIG. 3. (a) Left: topography image of the hybrid junction taken with the MB-modified probe. Right: schematics of the scanned area in relation to the whole nanostructure. (b) Left: SGM images of the transversal resistance over the junction at a fixed height of 200 nm. Green arrow indicates direction of the magnetization in the Py. Right: schematics of the SGM experiment. (c) Simulated spatial distributions of magnetization for different positions of the MB along the Au contact at h = 100 nm with centre of the bead at: (I) -450nm; (II) 0 nm; (III) +450 nm. Color disk indicates the direction of the magnetization inside the Py.

The influence of the MB stray field on the magnetization configuration in the nanowire is depicted in Fig. 3(c), which reports the magnetization spatial distribution for three different positions of the MB in respect to the Py wire, considering a height of 100 nm. When the MB is close to one side of the nanowire, *e.g.* x = ±450 nm, (where x = 0 corresponds to the center of the wire, Fig. 3(c) I, III), the MB's stray field produces a local deviation of the magnetization distribution leading to an angle η between magnetization and current density vectors different from zero. This results in an increase or decrease in the resistance depending on the sign of sin(2η), which reaches the maximum amplitude when the MB stray field causes a rotation of the magnetization in the Py nanowire of 45°, without effects of compensation between the stray field lines pointing in opposite directions. For the given bead/device geometry and vertical separation, this happens for x ~ ±450 nm. When the MB is exactly over the centre of the nanowire (Fig. 3(c) II), its stray field is responsible for a symmetric distribution of the magnetization in the nanowire, *i.e.* areas of both positive and negative contributions to the resistance, resulting in a zero overall change in the resistance.

C. Sensing volume

By scanning at different heights, it is possible to estimate how far the interaction between the MB and the hybrid junction extends, *i.e.* to define spatial and volume sensitivity of the junction.[23]

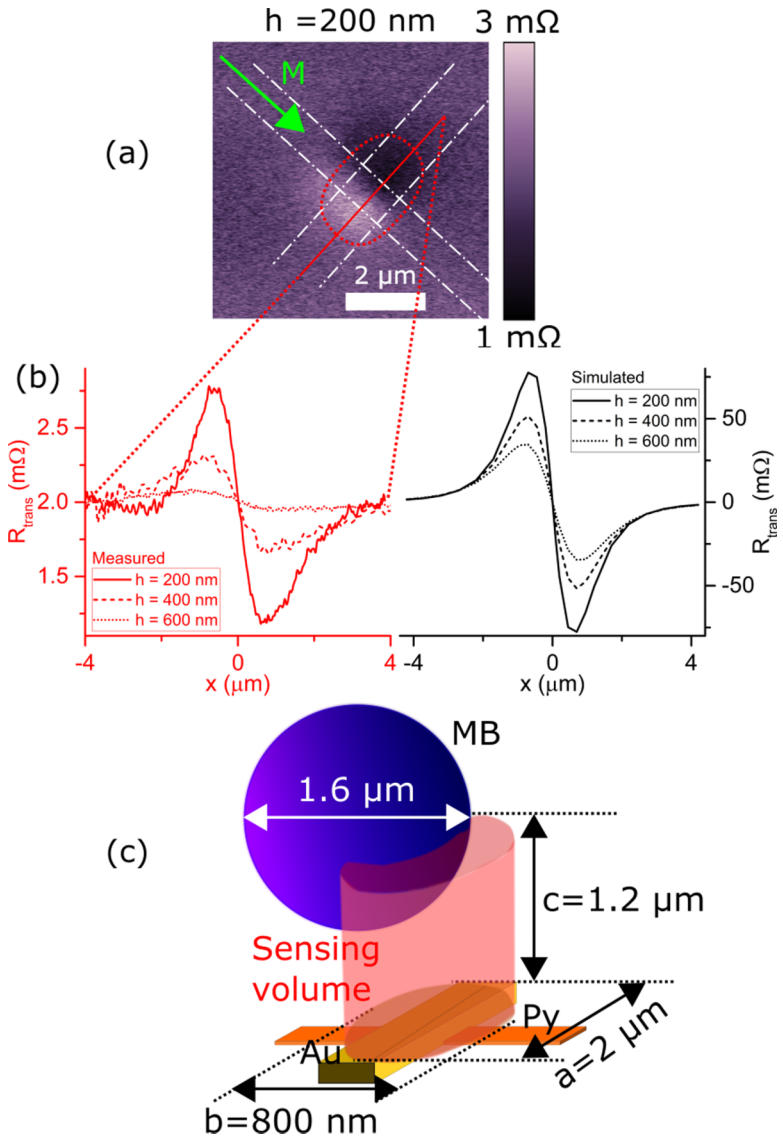

FIG. 4. (a) SGM map of transversal resistance at h = 200 nm. Green arrow indicates the direction of the magnetization. Red area indicates boundary where the signal meets the Rose criterion. (b) Left: Cross section taken from (a) and compared with measurements taken at different heights. Right: Cross sections extracted from simulations. (c) Schematics of the sensing volume (not in scale).

Figure 4(a) shows the transversal resistance taken at h = 200 nm. Applying Rose criterion for signal-to-noise detection,[35] we assume the effectiveness of MB sensing when the signal (positive or negative change in respect to background resistance) to noise ratio is higher than 5 (red contour in Fig. 4(a)). Following this criterion, the effect of the MB cannot be distinguished from the background signal for heights higher than 400 nm (Fig. 4(b) left shows cross sections of the transversal resistance taken at different heights), which can be assumed as the maximum distance between bottom of the MB and top of the junction guaranteeing reliable detection. By applying the same rule for the lateral distance, one can roughly estimate the sensing volume (*i.e.* the volume where the centre of the MB has to be located to allow detection) as an elliptical cylinder of volume about 1.51 μm^3 with dimensions c = 1.2 µm (height), a = 2 µm (along the Au wire) and b = 800 nm (along the Py wire) (see Fig. 4(c)). This result is similar to the sensing volume reported for DW-based devices made of Py.[23] For the DW-based devices (75 nm wide Py corner), based in longitudinal resistance

measurements instead of transversal, the SGM experiment with same type of MB achieved a conical sensing volume of 880 nm diameter of the base by 1.2 μm in height.[36]

When comparing the measured cross sections (Fig. 4(b) left) with results from the simulation (Fig. 4(b) right), the modeled resistance results are about 100 times higher than the measured one, since they correspond to the transverse resistance in the Py nanowire due to the PHE effect, while the measured ones are extracted from the Au contact (the electrical resistivities of Au and Py differ by a factor of 10-15). Hence it is expected that by increasing the resistivity of the overlying metal wire the value of the transversal resistance will increase, allowing much bigger sensing volume.

IV. CONCLUSION

Hybrid ferromagnetic (Py)/non-magnetic metal (Au) junctions (w = 400 nm) have been studied by means of magnetotransport measurements, SGM imaging with a MB attached to the scanning probe as well as micromagnetic simulations combined to a magnetotransport model, which includes both AMR and PHE phenomena. The transversal resistance across the nanowire shows an angular dependence with in-plane applied field. In small fields and relatively large angles, the transversal resistance is linear with field. In the intermediate field range, the resistance shows steps associated with the magnetization reversal, followed by saturation in high fields. This behavior makes the junction a good sensor for small in-plane fields (0 – 10 mT). In particular, when the in-plane field is perpendicular to the Py wire, the response of the resistance is linear in the range -20 mT $<$ B $<$ 20 mT with a sensitivity of 0.46 Ω/T.

The SGM studies demonstrate that the junction can be used to detect NdFeB MBs with size of ~1 μm and above, and that the measured signal depends on the direction of magnetization in the Py. Micromagnetic and magnetotransport modelling accurately describes the experimental results based on the PHE in the Py wire.

Performing SGM measurements at different heights allows to estimate the sensing volume for a specific "sensor–bead" combination. In the example considered here, this sensing volume can be roughly approximated by an elliptical cylinder of volume about 1.51 μm^3 with dimensions 1.2 μm in height, 2 μm along the Au wire and 800 nm along the Py wire.

In conclusion, the proposed hybrid junctions can be used to measure small in-plane magnetic fields and, in particular, the fields created by single MBs, proving that the junction can be used as a single MB detector.

ACKNOWLEDGMENTS

This work has been jointly funded by EMRP and EMRP participating countries under Project EXL04 (SpinCal) and FP7 project NanoMag. We are very grateful to Tom Wren, James Wells and Nora Dempsey for help with experiments and useful discussions.

[1] M. Donolato, P. Vavassori, M. Gobbi, M. Deryabina, M.F. Hansen, V. Metlushko, B. Ilic, M. Cantoni, D. Petti, S. Brivio, and R. Bertacco, Adv. Mater. **22**, 2706 (2010).
[2] M. Monticelli, E. Albisetti, D. Petti, D. V Conca, M. Falcone, P.P. Sharma, and R. Bertacco, J. Appl. Phys. **117**, 17B317 (2015).
[3] L. Ejsing, M.F. Hansen, A.K. Menon, H.A. Ferreira, D.L. Graham, and P.P. Freitas, J. Magn. Magn. Mater. **293**, 677 (2005).
[4] H. Corte-León, P. Krzysteczko, H.W. Schumacher, A. Manzin, D. Cox, V. Antonov, and O. Kazakova, J. Appl. Phys. **117**, 17E313 (2015).
[5] T.Q. Hung, S. Oh, J.R. Jeong, and C. Kim, Sensors Actuators, A Phys. **157**, 42 (2010).
[6] G. Vieira, A. Chen, T. Henighan, J. Lucy, F.Y. Yang, and R. Sooryakumar, Phys. Rev. B **85**, 174440 (2012).
[7] M. Donolato, M. Gobbi, P. Vavassori, M. Leone, M. Cantoni, V. Metlushko, B. Ilic, M. Zhang, S.X. Wang, and R. Bertacco, Nanotechnology **20**, 385501 (2009).
[8] P. Vavassori, V. Metlushko, B. Ilic, M. Gobbi, M. Donolato, M. Cantoni, and R. Bertacco, Appl. Phys. Lett. **93**, 203502 (2008).
[9] P. Vavassori, M. Gobbi, M. Donolato, M. Cantoni, R. Bertacco, V. Metlushko, and B. Ilic, J. Appl. Phys. **107**, 09B301 (2010).
[10] H. Corte-León, V. Nabaei, A. Manzin, J. Fletcher, P. Krzysteczko, H.W. Schumacher, and O. Kazakova, Sci. Rep. **4**, 6045 (2014).
[11] F.W. Østerberg, G. Rizzi, A.D. Henriksen, and M.F. Hansen, J. Appl. Phys. **115**, 184505 (2014).
[12] K. Kim, S.R. Torati, V. Reddy, and S. Yoon, J. Magn. **19**, 151 (2014).

[13] M. Volmer and M. Avram, J. Magn. Magn. Mater. **381**, 481 (2015).
[14] B.D. Tu, L.V. Cuong, D.T.H. Giang, T.M. Danh, and N.H. Duc, J. Phys. Conf. Ser. **187**, 012056 (2009).
[15] H. Kim, V. Reddy, K.W. Kim, I. Jeong, X.H. Hu, and C. Kim, J. Magn. **19**, 10 (2014).
[16] A. Schuhl, F.N. Van Dau, and J.R. Childress, Appl. Phys. Lett. **66**, 2751 (1995).
[17] A.D. Henriksen, B.T. Dalslet, D.H. Skieller, K.H. Lee, F. Okkels, and M.F. Hansen, Appl. Phys. Lett. **97**, 5 (2010).
[18] C.D. Damsgaard, S.C. Freitas, P.P. Freitas, and M.F. Hansen, J. Appl. Phys. **103**, 5 (2008).
[19] M.S. Gabureac, L. Bernau, G. Boero, and I. Utke, IEEE Trans. Nanotechnol. **12**, 668 (2013).
[20] Y.C. Chang, C.-R.C. Chang, I. Chang, J.C. Wu, Z.-H. Wei, and M.-F. Lai, J. Appl. Phys. **99**, 08B710 (2006).
[21] B.T. Dalslet, M. Donolato, and M.F. Hansen, Sensors Actuators A Phys. **174**, 1 (2012).
[22] M. Donolato, B.T. Dalslet, C.D. Damsgaard, K. Gunnarsson, C.S. Jacobsen, P. Svedlindh, and M.F. Hansen, J. Appl. Phys. **109**, 064511 (2011).
[23] H. Corte-León, B. Gribkov, P. Krzysteczko, F. Marchi, J.-F. Motte, H.W. Schumacher, V. Antonov, and O. Kazakova, J. Magn. Magn. Mater. 1 (2015), DOI: 10.1016/j.jmmm.2015.07.116.
[24] M. Megens, F. de Theije, B. de Boer, and F. van Gaal, J. Appl. Phys. **102**, 014507 (2007).
[25] Magnequench, January 8, 2009 (2009).
[26] *Note: Whereas in our previous work [Ref. 23] the moment was estimated from the manufacturer spreadsheet [Ref. 25], in the present manuscript we directly measured the magnetic moment for an array of beads using a SQUID magnetometer. Additionally, while in the previous work we used the bulk value of density for NdFeB, in the present work we provide a more realistic value by using a density in the range given by the manufacturer for the apparent density*.
[27] O. Bottauscio and A. Manzin, J. Appl. Phys. **115**, 17D122 (2014).
[28] A. Manzin and O. Bottauscio, IEEE Trans. Magn. **48**, 2789 (2012).
[29] A. Manzin and O. Bottauscio, J. Appl. Phys. **108**, 093917 (2010).
[30] T.R. McGuire and R.I. Potter, IEEE Trans. Magn. **MAG-11**, 1018 (1975).
[31] K.J.M. Eijkel and J.H.J. Fluitman, IEEE Trans. Magn. **26**, 311 (1990).
[32] A. Manzin, V. Nabaei, H. Corte-León, O. Kazakova, P. Krzysteczko, and H.W. Schumacher, IEEE Trans. Magn. **50**, 1 (2014).
[33] L.K. Bogart and D. Atkinson, Appl. Phys. Lett. **94**, 042511 (2009).
[34] G. Boero, M. Demierre, P.-. a. Besse, and R.S. Popovic, Sensors Actuators A Phys. **106**, 314 (2003).
[35] A. Rose, *Vision: Human and Electronic* (Plenum Press, New York, 1973).
[36] *Note: We Would like to stress that both cylindrical and conical shapes can be used for the description of the sensing volume. They both are only rough approximations to the real sensing volume. A more accurate description of the sensing volume would require mapping of sensitivity at each scanning height and definition of the detection area in each image according to the Rose criterion. These results would show a sensing volume with a bell-like shape (i.e. close to a cone when the bell is narrow and similar to a cylinder for a wide bell). Based on the large surface area in the present work, we approximate the shape by a cylinder*.